www.czasopisma.pan.pl PAN www.journals.pan.pl
Chemical and Process Engineering 2020, 41 (2), 143–163
DOI: 10.24425/cpe.2020.132537

Computational fluid dynamics modelling of short time bottle filling process

Monika Jałowiecka, Łukasz Makowski*

Warsaw University of Technology, Faculty of Chemical and Process Engineering, ul. Waryńskiego 1, 00-645 Warsaw, Poland

Every change in the bottle geometry as well as every change of physical and rheological properties poses a risk of excessive gas entrainment during a filling process. To maintain satisfactory filling efficiency there is a need to optimise this process with respect to all adverse phenomena which affect the fluid flow, such as spluttering on the bottom, air caverns formation and air entrainment with incoming liquid. This paper comprises numerical simulations of two filling methods. The first method involves dosing with a pipe placed over the free liquid surface of a fully filled bottle. The second method covers filling with a pipe located near the bottom. Moreover, the influence of rheological properties and surface tension values is considered. The comprehensive analysis of amount of entrained air represented by air volume fraction in dispensed liquid let the authors define the influence of filling speed on the mechanism and amount of entrapped air.

Keywords: air entrainment, bottle filling, Computational Fluid Dynamics, multiphase flow, Volume of Fluid method

1. INTRODUCTION

Bottled products are present in various branches of industry such as food, cosmetics and pharmaceutical industry. They must meet many requirements not only related to quality of the product but also to bottle attractiveness, recyclability, freshness guarantee and compliance of the product volume with the label. When the new product is introduced into the production line or there is a change in the bottle design it is necessary to optimise a filling process tailored for the new fluid or geometry due to the risk of excessive foaming, which can lead to inadequate filling, deterioration of product appearance and contamination of the outside of the labelled bottle.

The filling process may be conducted in miscellaneous ways. The common method is filling a bottle with a nozzle (Matice, 1997). The velocity of a thinning liquid jet impinging onto free liquid surface is a crucial factor that influences air entrainment. Bińi (1988) distinguishes three factors that are related to jet disturbances, minimum air entrainment velocity, jet diameter and its break-up length. The latter parameter is dependent on the type of considered jet region: laminar, turbulent or Weber. If the break-up of the jet occurs, droplets falling on the free liquid surface form cavities and lead to air entrainment. In the other case, coherent jet that reaches the pool surface creates a plunging point. Boualouache et al. (2018) mentioned an air boundary layer, which pulled down by interfacial shear also contributed to aeration process. Zhu et al. (1999) emphasise specificity of critical Reynolds numbers for air entrainment in terms of their

* Corresponding author, e-mail: lukasz.makowski.ichip@pw.edu.pl

applicability to exact nozzle design that influences the surface disturbances which directly lead to bubble formation.

As the velocity increases the cavity in free liquid surface also increases leading to the onset of air film formation around the plunging point and further unstable air film area, from which bubbles are entrained. The lower the viscosity of the liquid, the shorter the length of the stable air film (Biń, 1988). In another paper of Biń (1993) the subject of bubble size distribution, their residence time and the maximum depth, to which they can be entrained by the plunging jet, was discussed with comprehensive review of empirical correlations.

When high viscosity fluids are considered and the Reynolds number is below 1.2 there can occur some instabilities in jet flow like coiling and buckling (Roberts and Rao, 2011). These phenomena have an unfavourable impact on the filling process owing to the risk of air entrapment and incomplete filling (Ren et al., 2011). From a simulation perspective, it also prevents one from assuming an axisymmetric filling (Roberts and Rao, 2011). To define threshold for buckling Cruickshank (1998) studied the effect of H/D ratio (height of a nozzle position over its diameter). He proposed a condition that the Reynolds number should be smaller than 0.56 when $H/D > 3\pi$ to observe buckling.

Surface tension is also a valid factor in filling process. The higher surface tension, the more energy is required to form a bubble and the liquid has lower foaming tendency. There are other dimensionless numbers besides the Reynolds number which connect the surface tension, inertial and gravitational force effects on air entrainment intensity. The Weber number is the ratio of inertial forces to surface tension and relates to the tendency of jet breaking up (Pai et al., 2009). The latter is the Froude number that describes a relation between inertial forces and weight of the fluid. Its value is a measure of free surface disturbances (Brandt et al., 2017).

Summing up, every change in the bottle geometry as well as every change of physical and rheological properties poses a risk of excessive air entrainment. While introducing a new product multiple tests induce financial losses due to production line downtime and in such a situation conducting virtual experiments has an advantage. Numerical simulations give an opportunity to track numerous parameters and to carry out many experiments simultaneously. The only limit is the computational cost. Therefore, Computational Fluid Dynamics (CFD) becomes an effective tool in selection of optimum process conditions for which there is neither negative influence on product appearance nor its expansion from the bottle with the maximum filling efficiency. It should be noted that computational fluid dynamics is also successfully used to model other processes related to the filling process, such as: aeration process using liquid gas reactors (Al-Anzi, 2020), analysis of the flow in ladles during tapping of steel furnaces (Laux et al., 2000) and pool filling process (Sanjay and Das, 2017).

The main point of the article is to consider the short time of filling the bottle and analyse what is the cause of air capturing. For this purpose, computational fluid dynamics was used with Finite Volume Method (FVM) approach and Volume of Fluid (VOF) model. The accuracy and reliability of this model was investigated by Boualouache et al. (2018) on the basis of three scale model validation by comparison with results of Chanson experiment (2004) and correlations for air entrainment rate proposed by Van de Donk (1981) and Biń (1993). Sanjay and Das (2017) also verified VOF model with satisfactory compliance using their experiment and simulation data. It is noteworthy that CFD simulations examine the interaction between plunging jet and quiescent pool, whereas this work is extended by consideration of rising free liquid surface during the bottle filling process. In the remaining part of this paper there are presented cases that vary in filling methods, fluid rheological and surface tension properties as well as in filling speed in order to make a comprehensive analysis of their influence on air entrainment that can cause foam formation. The assumed measure of this phenomenon is the change of the fraction of air volume in the dosed liquid over time.

2. GEOMETRY AND NUMERICAL APPROACH

The geometry of a real 850 ml bottle (Fig. 1) was implemented into Ansys Fluent software. Since the calculation domain is axial-symmetrical, it was decided to perform calculations for half of the bottle in 2D. This simplification made it possible to create a more accurate calculation grid with a reasonable number of calculation cells, which consequently accelerated the calculation considerably. This solution was successfully used in previous works (Matice, 1997; Roberts and Rao, 2011; Tomé et al., 1999).

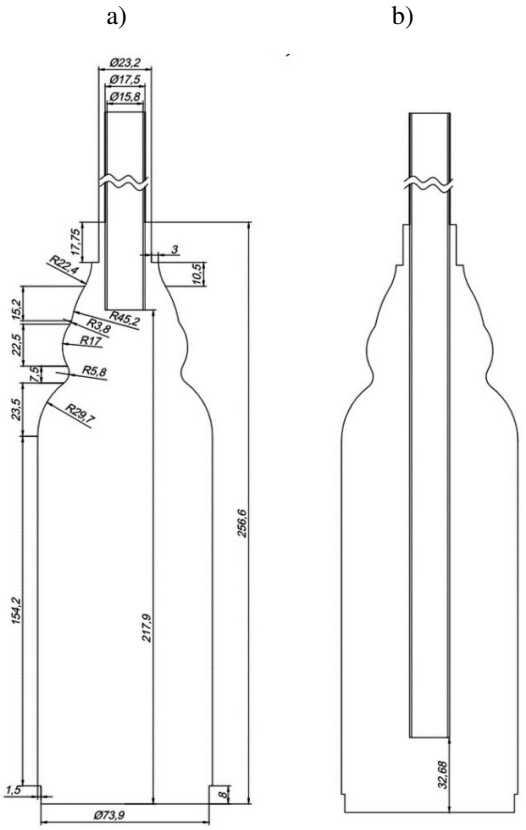

Fig. 1. Bottle geometry with dosing pipe in two locations, a) method 1 – the dosing pipe located above free liquid surface, b) method 2 – the dosing pipe located near the bottom of the bottle

A multi-block structured and conformal mesh was generated. The boundary layer was neglected because velocities near walls inside the bottle are very small due to high losses of kinetic energy caused by fluid collision with the bottom of the bottle and the following energy dissipation in already dispensed liquid. Geometry division into blocks and generated mesh are presented in Fig. 2 and mesh parameters are presented in Table 1.

Table 1. Parameters of generated mesh

Max. aspect ratio	Max. skewness	Min. orthogonal quality	Number of elements	Number of nodes
1.66	0.54	0.74	38837	39709

In every simulation it was assumed that at the beginning the bottle is filled with air, next the liquid flow inside the pipe is incompressible and the fluid flow inside the bottle is multiphase due to the presence of air bubbles. The Volume of Fluid (VOF) method was applied. Pressure-based flow with absolute velocity formulation influenced by gravitation was taken into consideration. Then boundary and initial conditions

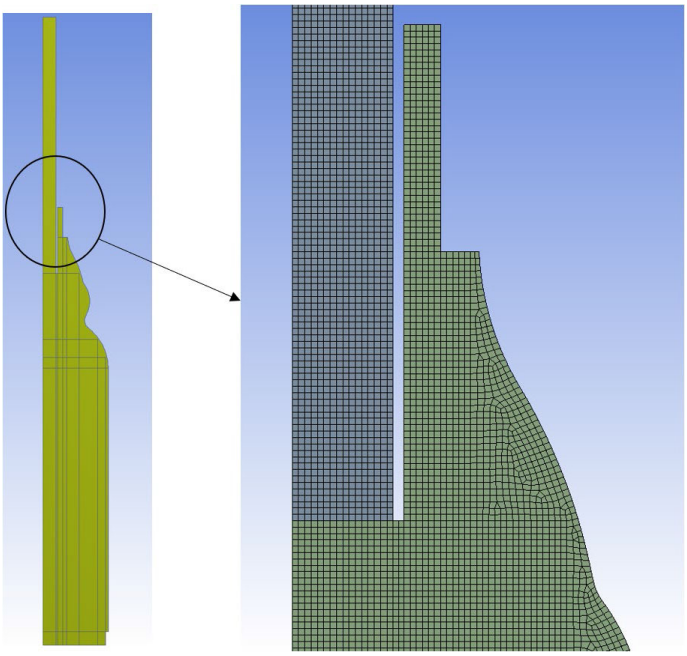

Fig. 2. An example of the density of the number grid in the geometry of the bottle

were defined as presented in Fig. 3. The inlet was specified as cross-section area of the pipe and the outlet was the annular space between the pipe and the bottle neck (the pressure at the outlet was 101325 Pa). The initial condition was that the dosing pipe was filled with liquid and the bottle was empty.

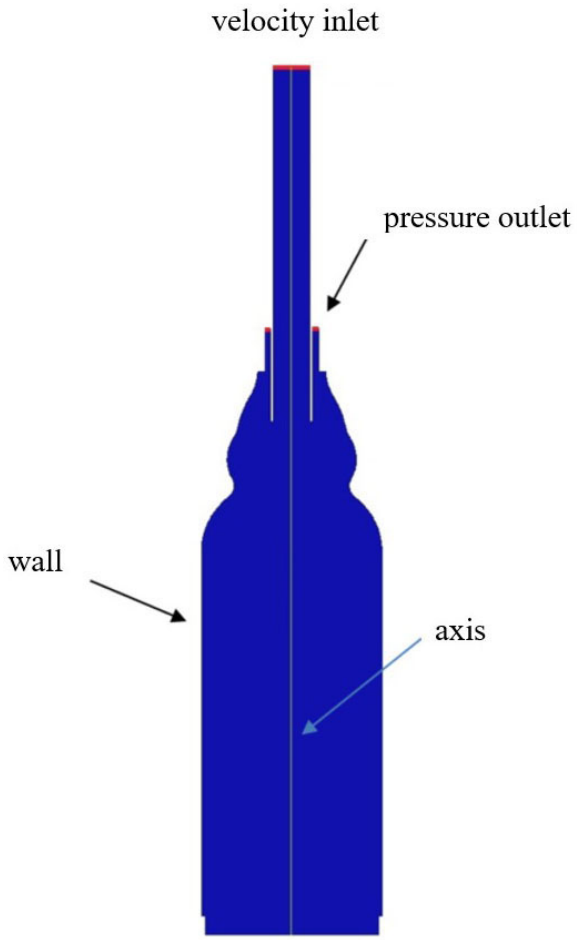

Fig. 3. Scheme of boundary conditions used in the calculation

Two characteristic real liquids were considered, which represent liquids of different viscosity range used in the filling process: water and depectinized grape concentrate. Both liquids were considered as Newtonian fluids in the temperature of 20°. Physical properties of the liquids are presented in Table 2. Flow regime in the dosing pipe was turbulent for water and laminar for grape concentrate, whose viscosity was much greater than that of water. Values of Reynolds number, Weber number and Froude number for each liquid and case are shown in Table 3. Laminar flow or k-ε turbulence model was applied depending on the Reynolds number. On can notice that in recent years, many works have been published presenting the possibility of using more advanced mathematical models, so called large eddy simulation (LES), to simulate practical processes (Makowski and Bałdyga, 2011; Makowski et al., 2012, Wojtas et al., 2020) or using direct numerical simulation (DNS) (Lahey Jr., 2009). They enable the simulation of processes in a wide range of Reynolds numbers. However, it should be remembered that such a solution increases both the calculation time and the demand for computing power many times and it is recommended to use it only in cases where the calculation results are significantly more accurate than the results obtained using lower-order models.

Table 2. Physical properties of water and grape concentrate in 20°, water properties from Venard and Street (1975); $\mu\rho$ of grape concentrate from Zuritz (2005) and σ from Bailey (2005)

Physical property	Water	Grape concentrate (67°Bx)
μ, Pa·s	0.001003	0.15026
ρ, kg/m^3	998.2	1337.3
σ, N/m	0.072	0.06

Table 3. Values of dimensionless Reynolds numbers $\mathrm{Re} = \frac{ud\rho}{\mu}$, Weber numbers $\mathrm{We} = \frac{\rho u^2 d}{\sigma}$ and Froude numbers $\mathrm{Fr} = \frac{u^2}{gh}$, where h is the height of nozzle position, d is nozzle diameter, Fr_1 and Fr_2 correspond to filling method 1 and 2

Q, ml/s	Q_{H_2O}, kg/s	$Q_{conc.}$, kg/s	u, m/s	Re_{H_2O}	$\mathrm{Re}_{conc.}$	We_{H_2O}	$\mathrm{We}_{conc.}$	Fr_1	Fr_2
100	0.10	0.13	0.51	8033	72	57	92	0.12	0.82
125	0.12	0.17	0.64	10041	90	89	144	0.19	1.28
166.67	0.17	0.22	0.85	13388	120	159	256	0.34	2.27

One can observe that the Froude numbers range from 0.12 to 2.27, it means then that in presented cases not only inflow Reynolds number is important, but also dimensionless length scale, h/d, influences the process. On the other hand, the values of the Weber number range from 57 to 256 which suggested that the inertial forces should dominate over the surface tension forces.

In this paper, 12 cases, presented in Table 4, differing in the dosed liquid and filling time were considered. Two dosing methods were also analysed. The first method (method 1) consisted in dosing the liquid with a tube placed above the free surface of a fully filled bottle. This is often a simple solution to avoid contamination of the outside of the liquid dosing tube. The disadvantage of this solution is the splash effect of the liquid, which can lead to large amounts of air being trapped and to foam. The second method (method 2) was to place the tube just above the bottom of the bottle. In this way, for most of the dosing time we are dealing with a dipped flow, which significantly reduces bubble entrainment. The geometry details of these methods are presented in Fig. 1.

Table 4. Scheme of boundary conditions used in the calculation

Case	u, m/s	Q, ml/s	τ, s	Method	Liquid
1	0.51	100	8.5	1	water
2	0.64	125	6.8	1	water
3	0.85	166.67	5.1	1	water
4	0.51	100	8.5	1	concentrate
5	0.64	125	6.8	1	concentrate
6	0.85	166.67	5.1	1	concentrate
7	0.51	100	8.5	2	water
8	0.64	125	6.8	2	water
9	0.85	166.67	5.1	2	water
10	0.51	100	8.5	2	concentrate
11	0.64	125	6.8	2	concentrate
12	0.85	166.67	5.1	2	concentrate

3. RESULTS

The industrial and practical interest in the filling process focuses primarily on increasing efficiency and thus the speed of filling containers. Therefore, one of the most important flow regimes in this process is the entrainment of air when the fluid is spluttering on the bottom of bottle or when the jet impact on liquid's free surface causes air bubble entrained in the liquid. For these reasons, the authors of the current work are interested in recognizing influence of filling speed on mechanism and amount of entrained air.

In the first cases, water dosing was considered in the velocity range of $0.51-0.85$ m s^{-1}, Re $= 8032-13388$) for the upper nozzle position (method 1). Figure 4 shows the distribution of water volume fraction during

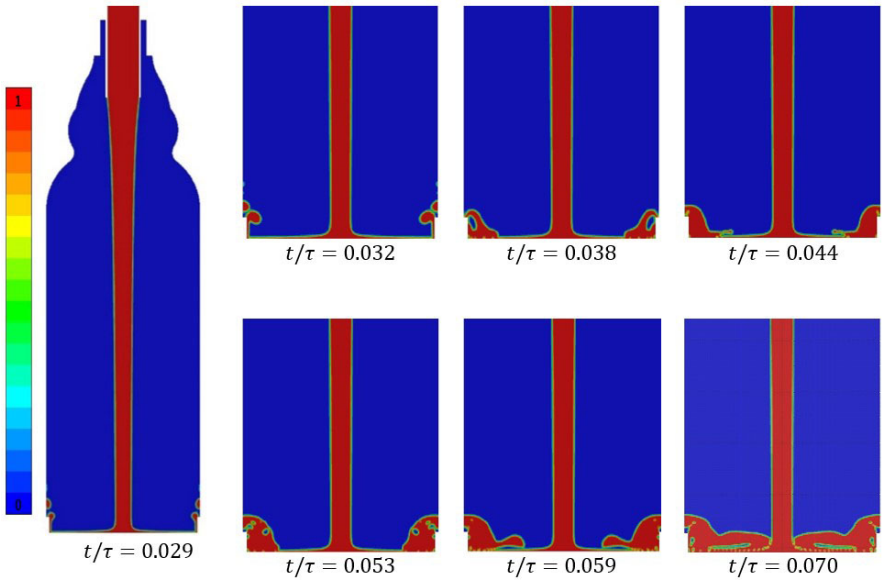

Fig. 4. Distribution of water volume fraction for $u = 0.51$ ms^{-1}, Re $= 8032$, filling method 1, first steps of the process

the first stage of process for $u = 0.51$ ms^{-1}. High value of air volume fraction at the beginning of the process is the result of entrapment of a significant amount of air in small liquid volume. It is caused by falling of liquid from walls in the axis direction.

One can notice that the real bottle used in modelling, has a bottom of smaller diameter than the main diameter of the bottle. That is why air bubbles accumulate on the annular surface at the height of the diameter change. At the beginning of the process the liquid hits the bottom and splashes over the surface, then rises on the walls and falls at two heights, just below and above the height of the diameter change. This moment is shown in Fig. 4 for $t/\tau = 0.032$. The liquid drops to the bottom, but the incoming stream is constantly rising on the walls causing another wave of liquid ($t/\tau = 0.053$). As a result, air caverns are created ($t/\tau = 0.070$), from which bubbles will form.

Further on in the filling process it is observed that bubbles are flowing to the bottom, where subsequently are flowing back up with the bounced off liquid (Fig. 5). Due to low dosing velocity bubbles are rising

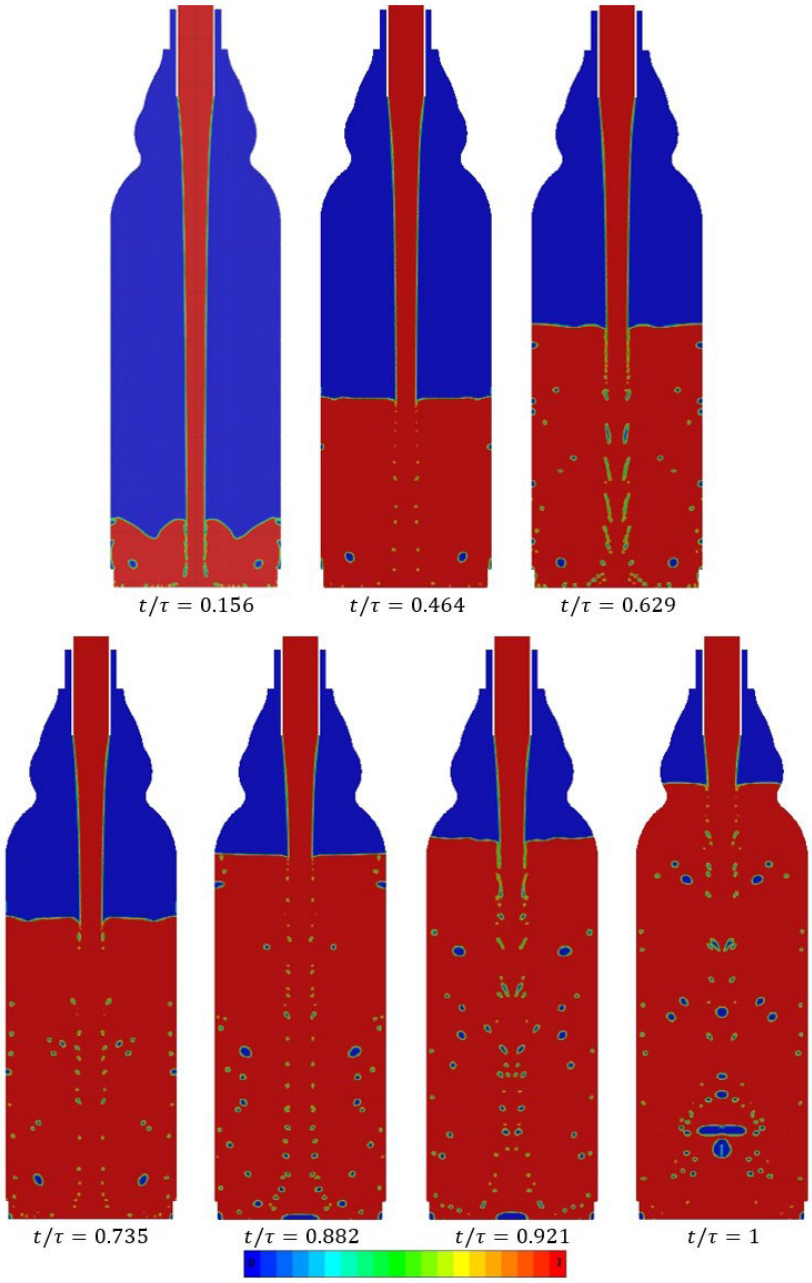

Fig. 5. Distribution of water volume fraction for $u = 0.51$ ms^{-1}, Re = 8032, filling method 1

slower than flowing down with incoming stream. When bubbles achieve the free surface of the liquid, they break up and decrease of air volume fraction is noticed. The regions with the highest vorticity are shown in Fig. 6. One can observe that the most favourable place for bubbles to adhere and coalesce in this case is the middle of the bottom. In the end of the process the largest bubble detaches from the middle of the bottom and flows to the surface.

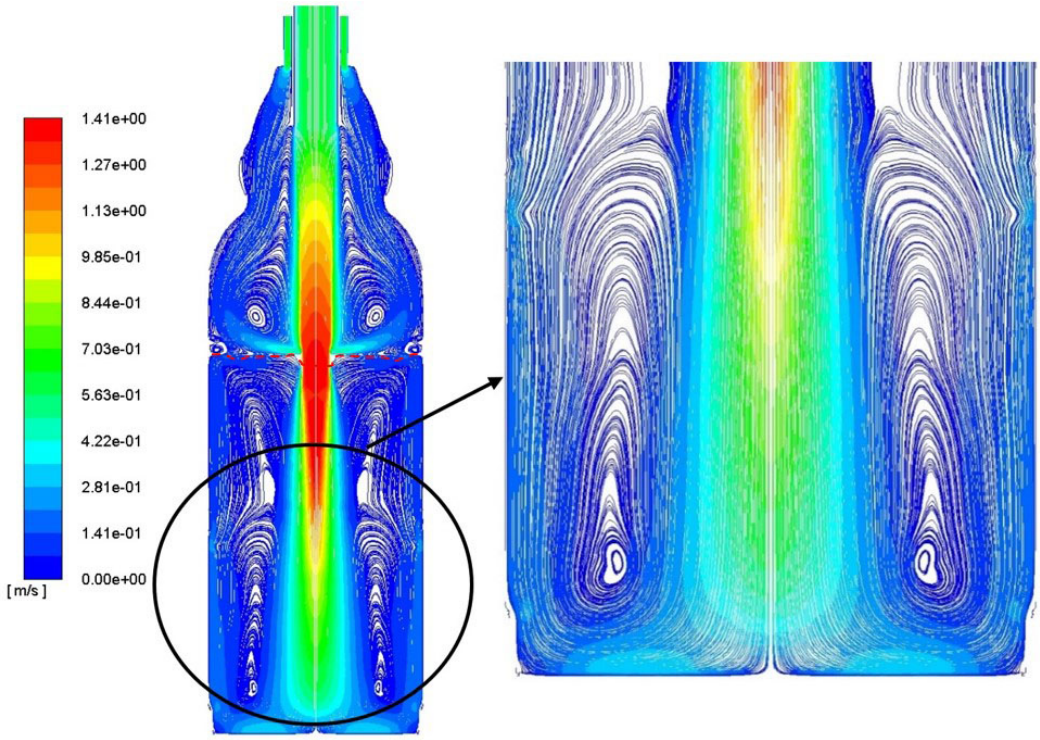

Fig. 6. Pathlines representing vorticity of multiphase flow for u = 0.51 ms^{-1}, Re = 8032, filling method 1, the free liquid surface is marked with red dashed line

The calculation results are summarised in Fig. 7 showing the change in the volume fraction of air retained in the liquid. The fraction is defined by the following equation:

$$X_{air}(t) = \frac{V_{air}(t)}{V_{liquid}(t)} \tag{1}$$

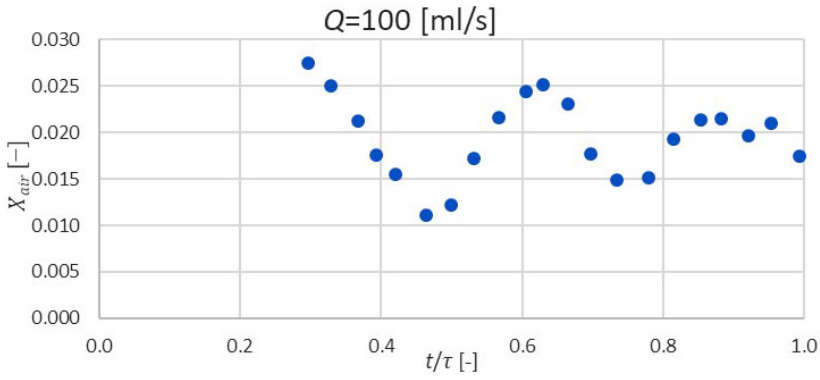

Fig. 7. Air volume fraction in water during the filling process, u = 0.51 ms^{-1}, Re = 8032, filling method 1

Note that the volume fractions of retained air are not large and take values from 0.01 – 0.03. This is different if the dosing velocity is increased (Fig. 8).

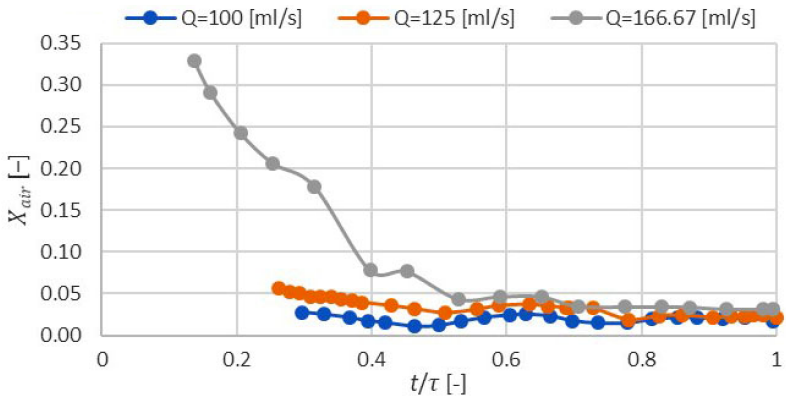

Fig. 8. Air volume fraction in water during the filling process, $u = 0.51-0.85$ ms^{-1}, Re = 8032−13388, filling method 1

It is clear that as the dosing rate increases, air retention in the liquid increases rapidly. Analysing case 2 one can see that after $t/\tau = 0.635$ progressive descend of frothing can be observed until a sudden decrease in value of air volume fraction in point $t/\tau = 0.781$. The reason of this change is release of the biggest bubbles, formed at the beginning of the process, which start rising in point $t/\tau = 0.635$. This is shown in Fig. 9. Similarly to case 1, here one notices that in the end of the process the dissipation of kinetic energy

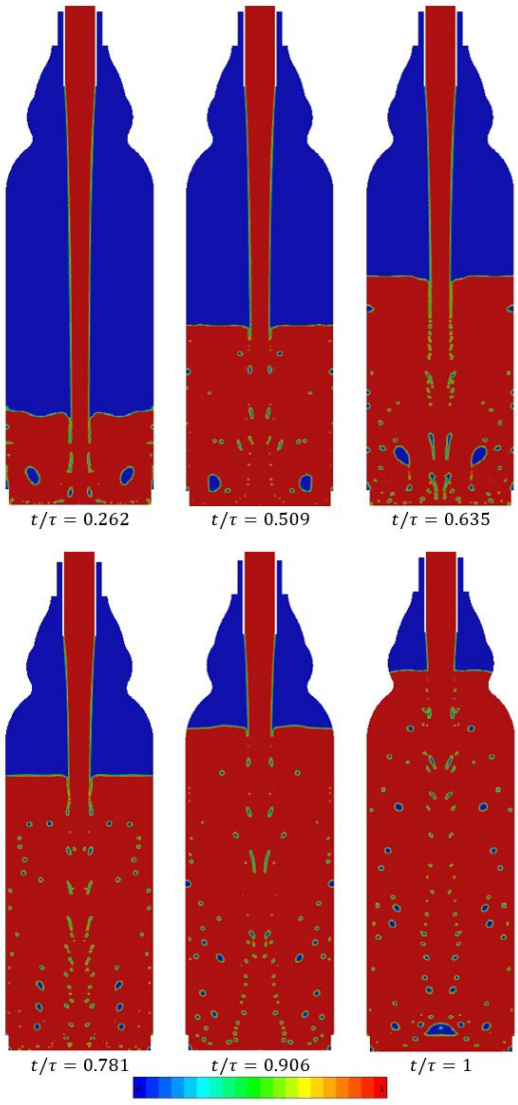

Fig. 9. Distribution of water volume fraction for $u = 0.64$ ms^{-1}, Re = 10041, filling method 1

along the height of the dispensed liquid is sufficient to let the bubbles coalesce in the middle of the bottom and then ascend to the surface. The difference between case 1 and 2 is that the bubbles are rising faster with water that turns back at the bottom and flows upwards in the second simulation. Therefore, air volume fraction oscillations in case 2 are smaller than in case 1.

In case 3 one can observe significantly higher values of air volume fraction than in simulations described beforehand. Figure 10 shows the volume fraction distributions for the highest stream. The initial flow of liquid reaching the bottom strongly entrainment air. The bubbles created in this way do not break down until half the dosing time. This phenomenon can lead to foam. The decline in air volume fraction values is faster and without oscillations. In the end of the process ($t/\tau = 1$, Fig. 11) air does not form large bubbles, but is dispersed into small bubbles.

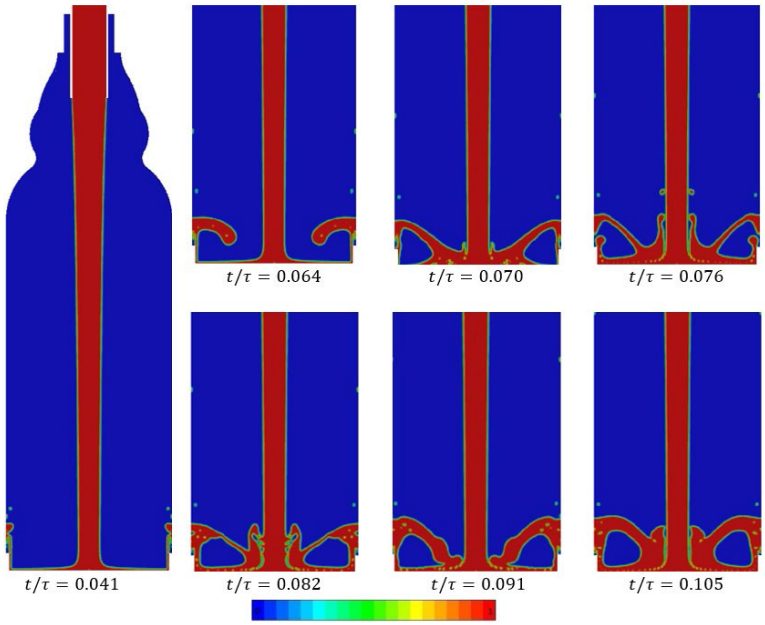

Fig. 10. Distribution of water volume fraction for $u = 0.85$ ms^{-1}, Re = 13388, filling method 1, first steps of filling process

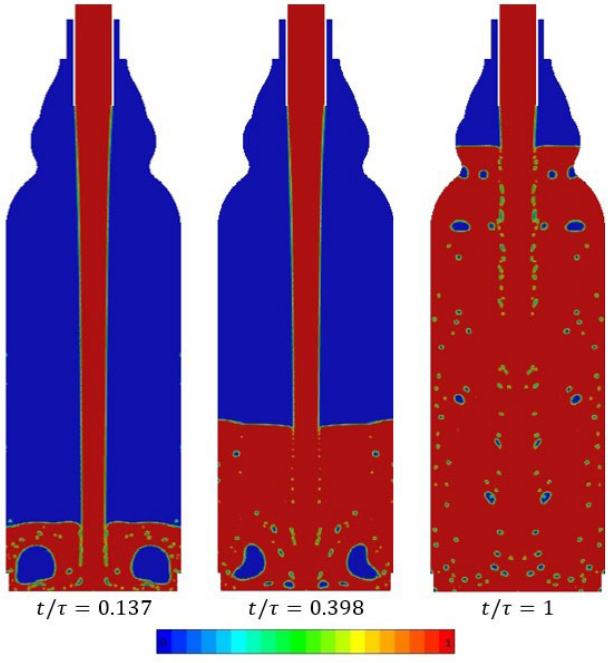

Fig. 11. Distribution of water volume fraction for $u = 0.85$ ms^{-1}, Re = 13388, filling method 1

Dosing the considered volume of low-viscosity liquids in 5 seconds may lead to strong air entrainment, but on the other hand it is a very attractive time from the practical point of view. Therefore, in the next stage the dosing of high viscosity liquid such as grape concentrate with a viscosity of 0.15026 Pa·s was considered. Liquid flow in the pipe is laminar due to the high dynamic viscosity of grape concentrate. Air bubbles will encounter more hydrodynamic drag and therefore lift slower to the free liquid surface. The frothing of the liquid will last longer than in water.

At the beginning of the process the concentrate gradually froths between points $t/\tau = 0.07$ and $t/\tau = 0.156$ owing to the greater air entrainment with incoming liquid than bubbles release at the surface (Fig. 12). A rapid decline of air amount is observed shortly after two large bubbles reached the free liquid surface and burst. The thing is similar in further oscillations (Fig. 13). It is worth pointing out that more bubbles are formed in grape concentrate than in water because of lower surface tension of the concentrate. Air volume fraction value decreases constantly towards the end of the process after point $t/\tau = 0.612$ in Fig. 13.

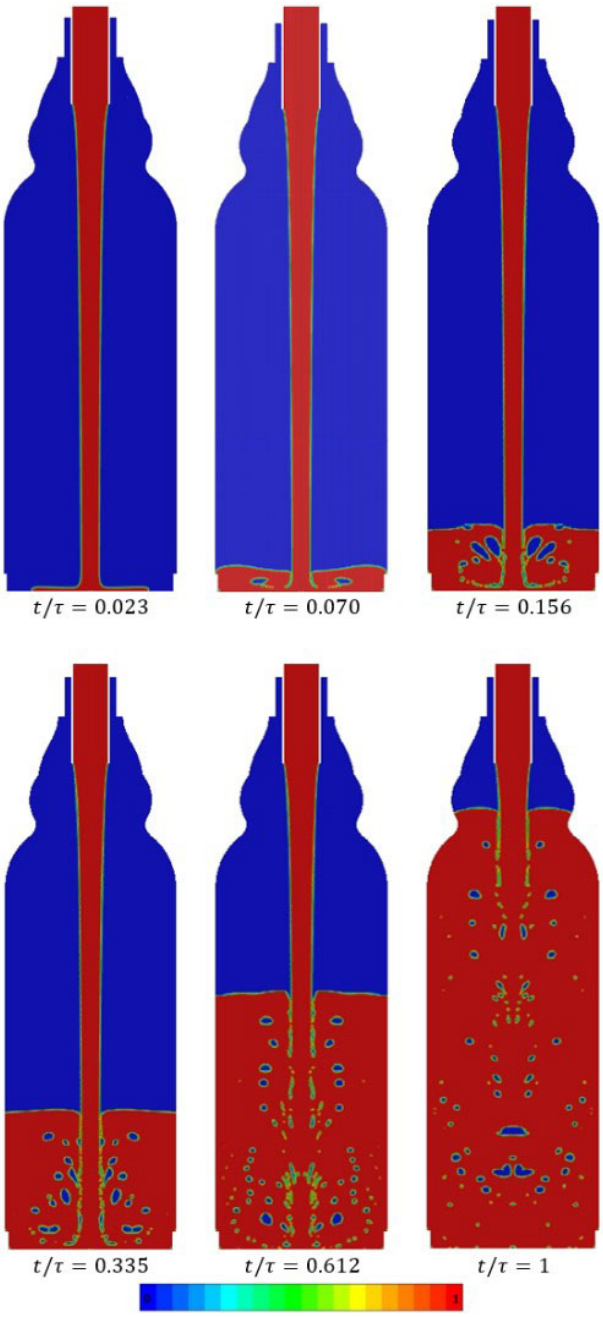

Fig. 12. Distribution of grape concentrate volume fraction for $u = 0.51$ ms^{-1}, Re = 72, filling method 1

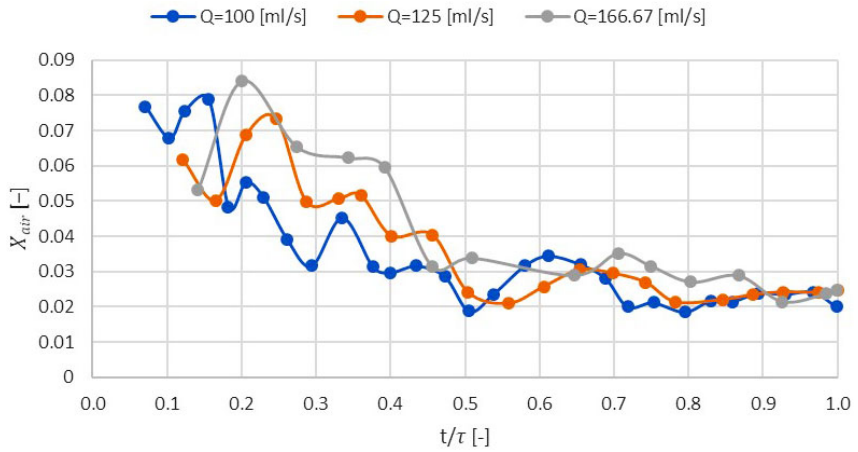

Fig. 13. Air volume fraction in grape concentrate during the filling process, u = 0.51–0.85 ms^{-1}, Re = 72–120, filling method 1

Interestingly, as the flow rate increases, there is no increased entrainment during the process. Analysing Fig. 13 one can observe that the volume fraction of air in the concentrate is at the maximum level of 0.08 - 0.06 and is almost constant as a function of dosing time. On the other hand, for higher filling times the fraction of air contained in the water during the process is lower than for the concentrate. This is, of course, due to higher viscosity, which reduces the lifting speed, but also significantly reduces bubble breakage.

Analysing the volume fraction distributions for water and concentrate one can observe that the air bubble captured in the first moment of filling moves differently in both cases. In the case of water, it is pushed against the wall and moves upwards along circulation paths. In the case of higher viscosity liquids, the pressure force pushes the bubbles towards the axis of the bottle, where it contacts the incoming stream which, with its energy, causes the bubbles to break down. This phenomenon is clearly visible in Fig. 14.

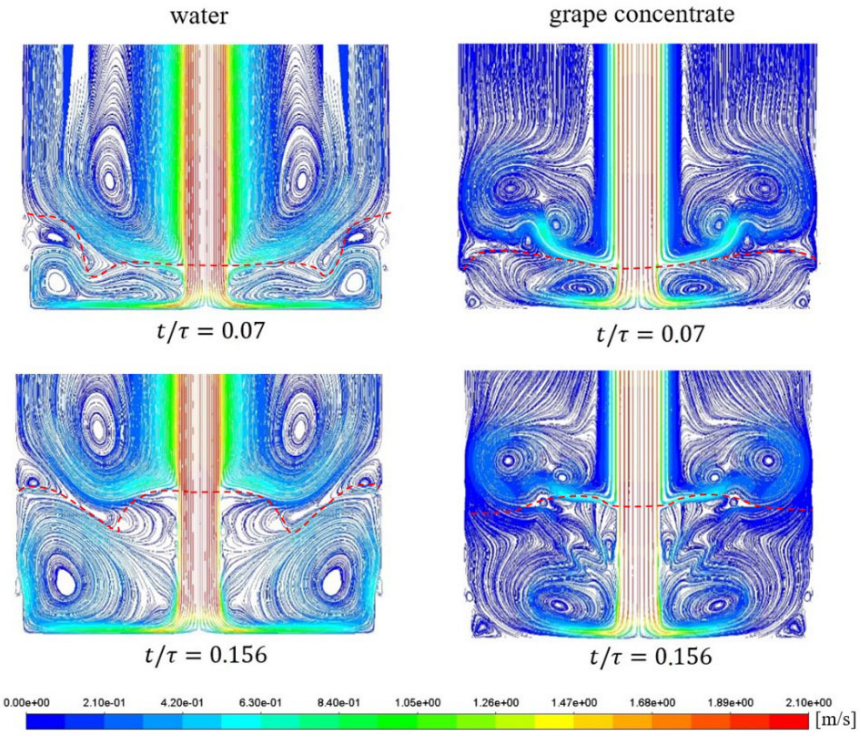

Fig. 14. Pathlines representing vorticity of multiphase flow, u = 0.51 ms^{-1}, filling method 1, free liquid surface is marked by a red dashed line

In the case of water, the circulation loop is formed at the bottom of the bottle and extends over the entire width for both $t/\tau = 0.07$ and $t/\tau = 0.156$ and represents inertia-convection mixing. In this case, the bubble captured near the dosed stream will flow towards the wall, where it will reach the area of lower velocity, allowing it to rise upwards as the energy of the circulation loop decreases due to the rise of the liquid level.

In the case of concentrate, the circulating loop created is much smaller and covers the area near the dosed stream, while a dead zone is created near the container wall. The resulting bubble is turned around near the jet, which makes it impossible to lift it. This can be seen in Fig. 15 (for $Q = 166.7$ ml/s) for $t/\tau = 0.137$ where the gas bubble is broken up by many smaller, rotating in the circulation loop shown in Fig. 16 (for $t/\tau = 0.137$). At the same flow, the primary gas bubble in the water retains the same size and only at a later step, under the influence of the mass of the liquid, it breaks up. This phenomenon will have a major influence on the formation of foam.

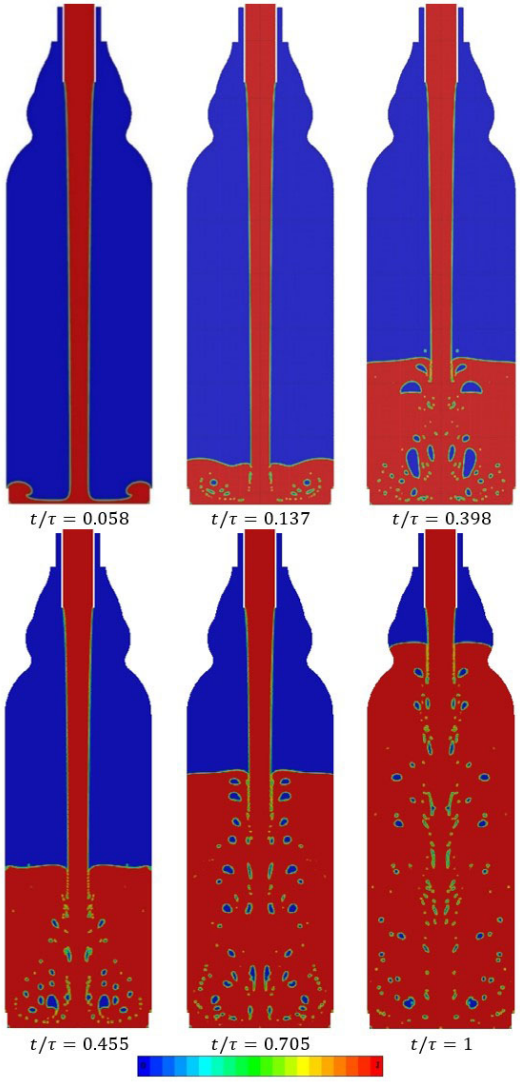

Fig. 15. Distribution of grape concentrate volume fraction, $u = 0.85$ ms^{-1}, Re = 13388, filling method 1

The most common solution to avoid strong aeration while maintaining high filling speeds is submerged filling. There are two solutions to this process, with a fixed dosing tube introduced into the container near the bottom and a tube that lifts up with the liquid after submerging. The second solution significantly reduces contamination of the dosing tube but is much more difficult and expensive to implement. The paper considers the first solution. Figures 17, 18, 19 show selected moments of water dosing for considered

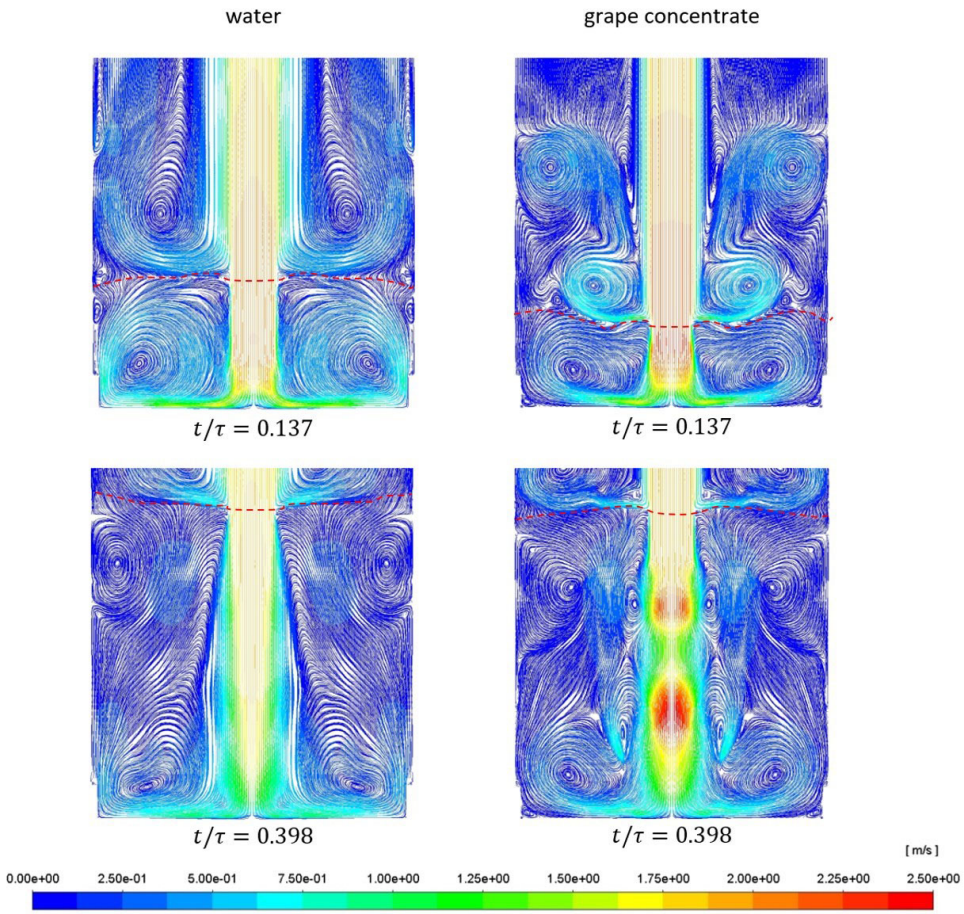

Fig. 16. Pathlines representing vorticity of multiphase flow, $u = 0.85$ ms^{-1}, filling method 1, free liquid surface is marked by a red dashed line

flows, while Fig. 20 displays the volume fraction of air during the process. It is clearly visible that the volume fraction of air is much lower than in the case of top dosing, especially for the highest stream, where the maximum volume fraction of air for method-2 is 5 times lower.

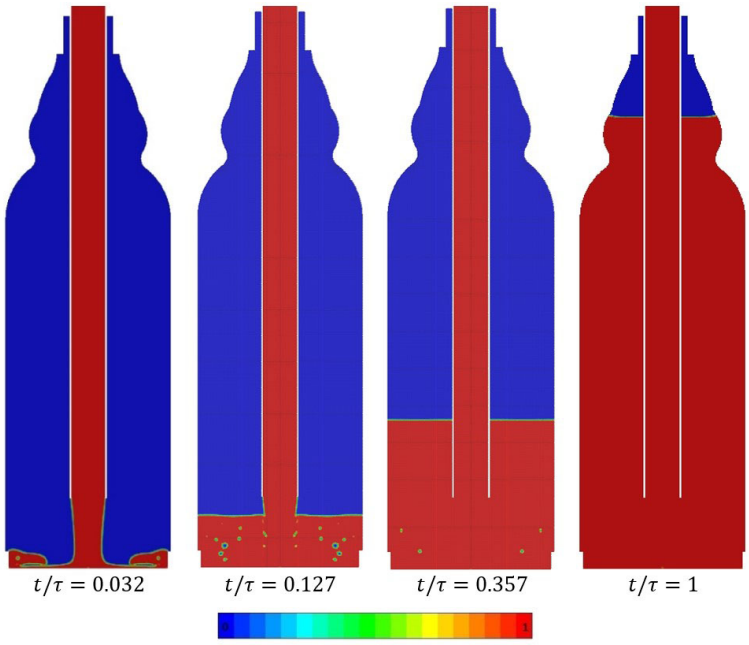

Fig. 17. Distribution of water volume fraction, $u = 0.51$ ms^{-1}, Re = 8033, filling method 2

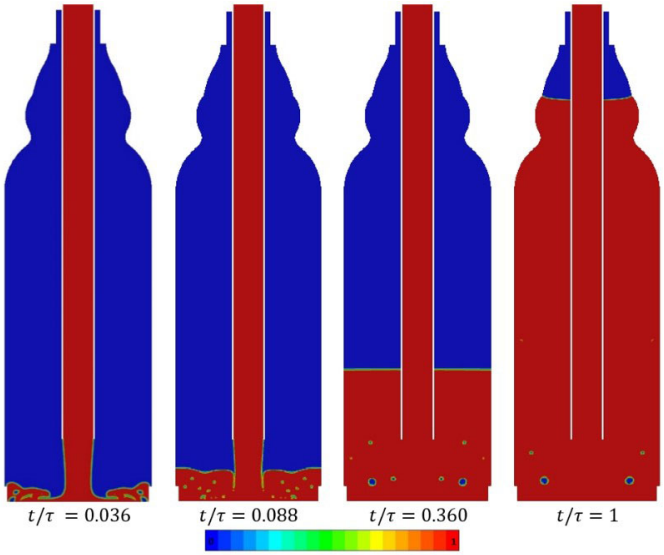

Fig. 18. Distribution of water volume fraction, u = 0.64 ms^{-1}, Re = 10041, filling method 2

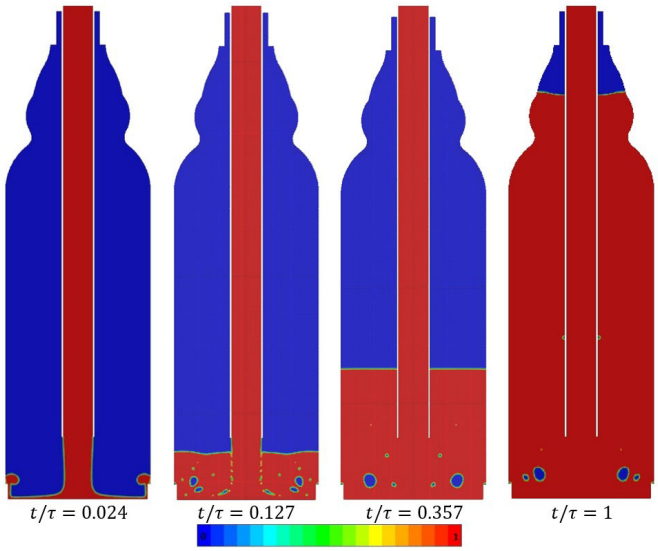

Fig. 19. Distribution of water volume fraction, u = 0.85 ms^{-1}, Re = 13388, filling method 2

Also the volume fraction of gas at the end of the dosing process is about 3 times smaller. Observing the volumetric distributions for the two higher streams of liquid you can see that after the initial filling

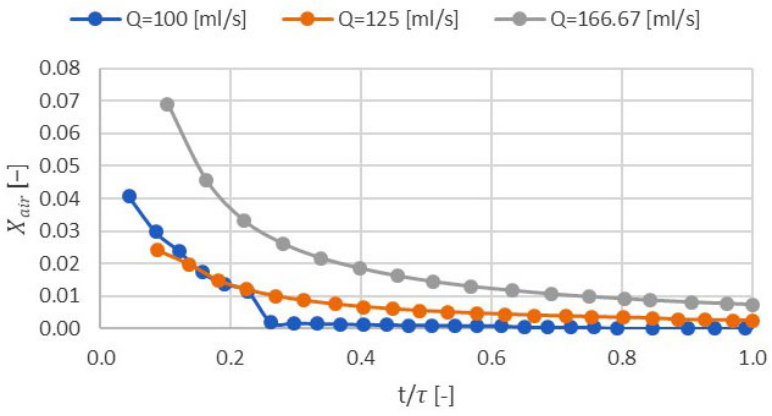

Fig. 20. Air volume fraction in water during the filling process, u = 0.51–0.85 ms^{-1}, Re = 8033–13388, filling method 2

stage (not submerged) there are single bubbles that remain in the same position until the end of the filling process, not lifting up. The same phenomenon is observed in the case of concentrate dosing (Figs. 21, 22, 23), where in the beginning of the filling process small bubbles flow upwards and burst. Some of them are coalescing and remain entrapped in the area of much vorticity near the bottom until the end of the process. Only when the bottle is filled and dosing is stopped the bubbles may ascend to the surface. This leads to a very similar volume fraction of air during the filling process as shown in Fig. 24.

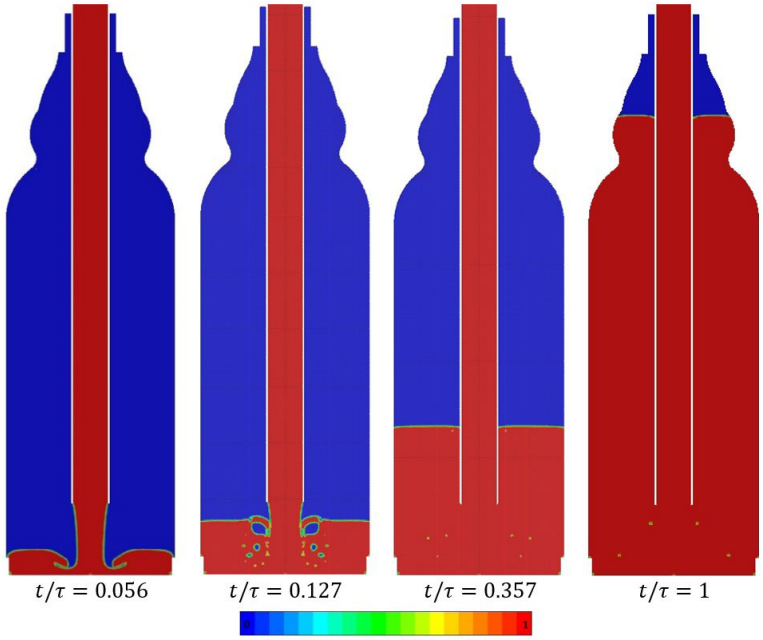

Fig. 21. Distribution of grape concentrate volume fraction, $u = 0.51$ ms^{-1}, Re = 72, filling method 2

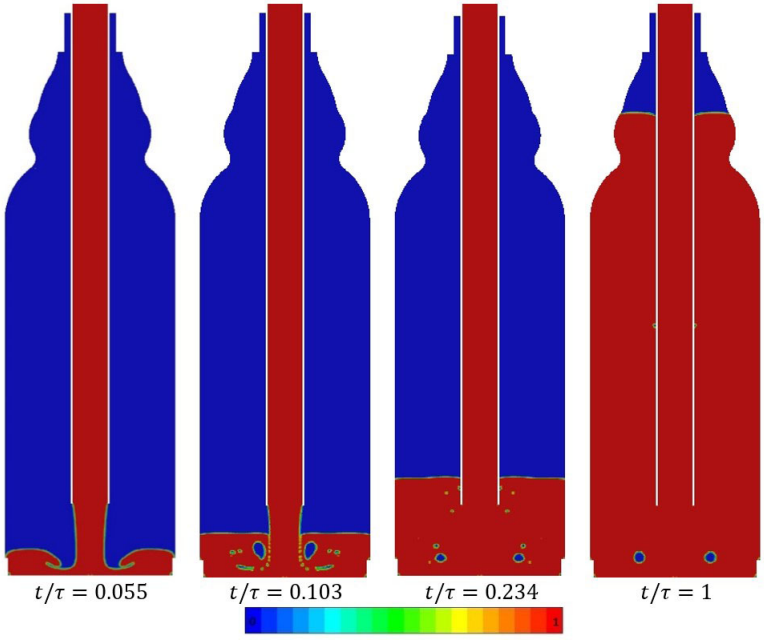

Fig. 22. Distribution of grape concentrate volume fraction, $u = 0.64$ ms^{-1}, Re = 90, filling method 2

Bubble retention can be explained by observing the shape of circulating loops for characteristic filling stages: before submerging for $t/\tau = 0.127$ and just after submerging for $t/\tau = 0.357$. Figure 25 presents a comparison of the stream line for the flow $Q = 100$ ml/s. For the first stage, the circulating loops formed are similar to those of method 1. In the case of water, the loop extends over the entire width of the bottle, and

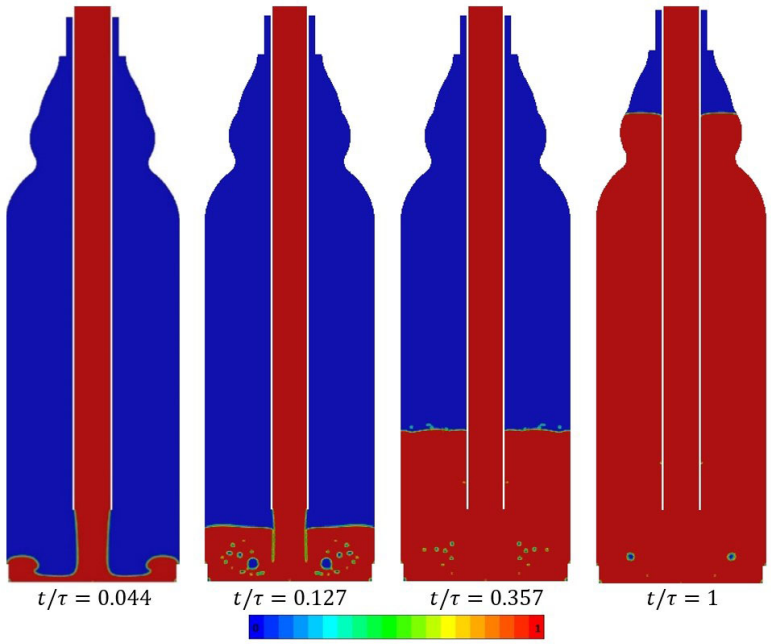

Fig. 23. Distribution of grape concentrate volume fraction, u = 0.84 ms^{-1}, Re = 120, filling method 2

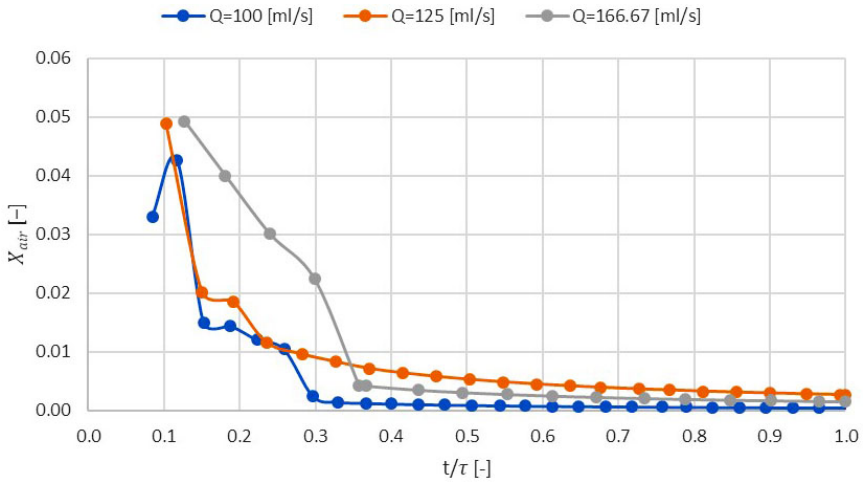

Fig. 24. Air volume fraction in grape concentrate during the filling process, u = 0.51–0.85 ms^{-1}, Re = 72–120, filling method 2

in the case of concentrate, it is located near the main stream. Then, for the second stage, for the submerged flow, one can see that the circulating loop is lower than that of the top dosing, without reaching the free surface. Of course, for liquids with a lower viscosity the circulation zone is larger because the energy of the dosed stream is more easily dissipated. Therefore, the bubble that is formed at the very beginning has the possibility to lift up until it is released on a free surface. For this reason, no visible bubbles are observed during the submerged dosing stage.

As the dosed flow rate increases, the situation becomes worse. The analysis of Fig. 26 shows that such a strong jet and a small distance from the bottom make the shape of circulation loops for water and concentrate similar. In both cases the formed bubbles are stopped in the area of their formation. However, in the submerged dosing stage the situation changes. In the water an area with strong internal swirls is created from which the bubble cannot escape until the end of the process. In the case of concentrate we have a situation similar to that of dosing at lower streams, where the bubble lifts up. Only small bubbles are left for which the buoyancy force is too low to rise to the surface during dosing.

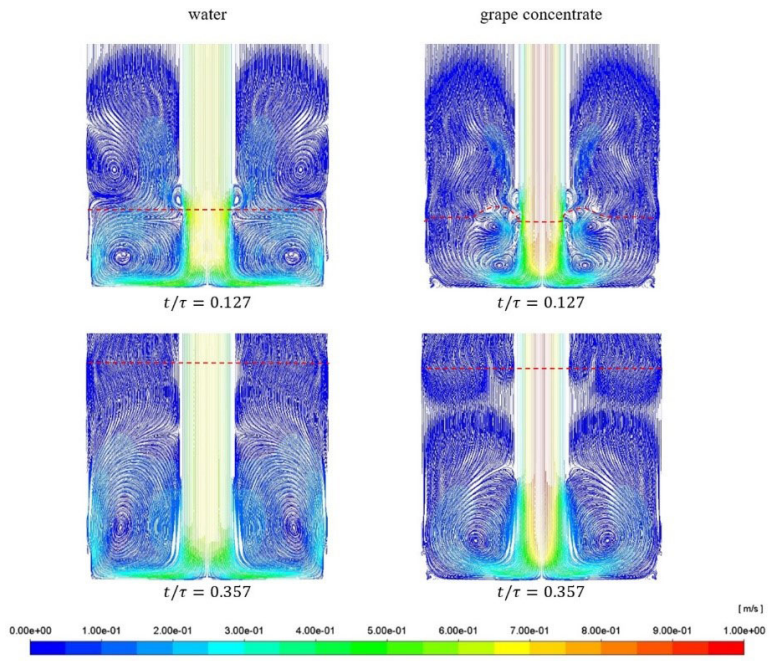

Fig. 25. Pathlines representing vorticity of multiphase flow, $u = 0.51$ ms^{-1}, filling method 2, free liquid surface is marked by a red dashed line

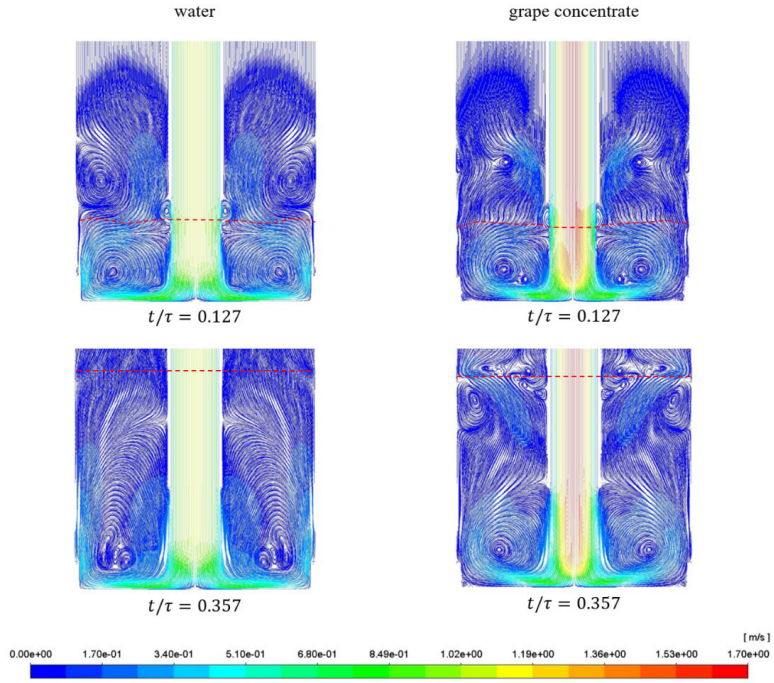

Fig. 26. Pathlines representing vorticity of multiphase flow, $u = 0.85$ ms^{-1}, filling method 2, free liquid surface is marked by a red dashed line

4. CONCLUSIONS

Within the scope of conducted CFD simulations of the filling process, the authors focus on determining changes in values of air volume fraction with respect to time in dispensed liquid considering two filling methods. The first method involves dosing the liquid with a pipe placed in the upper part of the bottle. The second method concerns filling with the pipe located near the bottom of the bottle. It enables to define the influence of specific dosing method on gas retainment process.

At the beginning of the filling process liquid that is being dosed is rising on the walls after reaching the bottom of the bottle. It is a crucial stage of the process, in which the most amount of air becomes entrapped in the liquid volume by a stream falling in the axis direction. In the analysed geometry the flat bottom of the bottle has a diameter smaller than the main diameter of the bottle by 3 millimetres. It is worth mentioning that tiny air bubbles gather in the area between the wall and the flat bottom. The other area which is favourable to the gathering of the bubbles is the annular space at the height of the expansion of the bottle diameter. Thus, it may be asserted that every region in which the wall forms a right angle with the base will be the place where bubbles retain. Hence the design of the bottle should not include rapid diameter changes. Additionally, in such an area bubbles coalesce, expand their size and accumulate in the axis of the bottom of the bottle. They detach from the bottom after the incoming stream dissipates the vast amount of kinetic energy along the height of dispensed liquid.

The examined bottle of 850 millilitre volume has considerable height. Following conducted simulations, the negative impact of dosing the liquid from a high position was observed in comparison to the results from simulations of method 2. The method that involves filling the bottle with the pipe that remains above the free liquid surface during the whole process is frequently used in industry when it is undesirable to immerse the dosing pipe because of the risk of contamination of a label or the area of the bottle neck that has to be sealed, especially in case of filling the bottle with high viscous liquid which may remain on the pipe walls for a long time. Therefore, a better approach to fill such large bottles would be introducing a moveable nozzle over the bottom of the bottle and rising it with the increasing height of the free liquid surface.

For dosing velocities of 0.51 m/s and 0.64 m/s noticeable oscillations of air volume fraction values are observed over time when method 1 is applied. It is caused by considerable difference between velocities of bubbles rising to the free liquid surface and bubbles that are being entrained within incoming stream downwards. If the bottle had been lower, then the oscillations would not have been so noticeable.

Entrapment of the largest air bubbles is observed for both methods in the areas of the highest vorticity in which a change in flow direction occurs in a consequence of stream collision with the bottom.

SYMBOLS

Q	flow rate, ml/s
u	inlet velocity, m/s
$V_{air}(t)$	instantaneous volume of air retained in the liquid, m^3
$V_{liquid}(t)$	instantaneous volume of liquid during the filling process, m^3

Greek symbols

μ	dynamic viscosity, Pa·s
ρ	density, kg/m^3
σ	surface tension, N/m
τ	filling time, s

REFERENCES

Al-Anzi B.S., 2020. Effect of primary variables on a confined plunging liquid jet reactor. *Water*, 12, 764. DOI: 10.3390/w12030764.

Bailey A.F.G., 2005. *The concentration of aqueous solutions by osmotic distillation (OD)*. MSc thesis, Queensland University of Technology.

Biń A.K., 1988. Minimum air entrainment velocity of vertical plunging liquid jets. *Chem. Eng. Sci.*, 43, 379–380. DOI: 10.1016/0009-2509(88)85051-6.

Biń A.K., 1993. Gas entrainment by plunging liquid jets. *Chem. Eng. Sci.*, 48, 3585–3630. DOI: 10.1016/0009-2509(93)81019-R.

Boualouache A., Zidouni F., Mataoui A. 2018. Numerical visualization of plunging water jet using Volume of Fluid Model. *J. Appl. Fluid Mech.*, 11, 95–105. DOI: 10.29252/jafm.11.01.27861.

Brandt M.J., Johnson K.M., Elphinston A.J., Ratnayaka D.D., 2017. *Twort's Water Supply*. 7th edition, Butterworth-Heinemann, 581–619. DOI: 10.1016/B978-0-08-100025-0.00014-4.

Chanson H., Aoki S., Hoque A., 2004. Physical modeling and similitude of air bubble entrainment at vertical circular plunging jets. *Chem. Eng. Sci.*, 59, 747–758. DOI: 10.1016/j.ces.2003.11.016.

Cruickshank J.O., 1988. Low-Reynolds-number instabilities in stagnating jet flows. *J. Fluid Mech.*, 193, 111–127. DOI: 10.1017/S0022112088002071.

Fellows P.J., 2009. *Food processing technology – Principles and practice*. 3^{rd} ed., Woodhead Publishing Limited and CRC Press LLC, Cambridge, 782–785. DOI: 10.1533/9781845696344.

Lahey Jr. R.T., 2009. On the direct numerical simulation of two-phase flows. *Nucl. Eng. Des.*, 239, 867–879. DOI: 10.1016/j.nucengdes.2008.06.020.

Laux H., Johansen S.T., Berg H., Klevan O.S., 2000. CFD analysis of the turbulent flow in ladles and the alloying process during tapping of steel furnaces. *Scand. J. Metall.*, 29, 71–80. DOI: 10.1034/j.1600-0692.2000.d01-8.x.

Makowski Ł., Bałdyga J., 2011. Large eddy simulation of mixing effects on the course of parallel chemical reactions and comparison with k-ε modeling. *Chem. Eng. Process. Process Intensif.*, 50, 1035–1040. DOI: 10.1016/j.cep.2011.06.003.

Makowski Ł., Orciuch W., Bałdyga J., 2012. Large eddy simulations of mixing effects on the course of precipitation process. *Chem. Eng. Sci.*, 77, 85–94. DOI: 10.1016/j.ces.2011.12.020.

Matice C.J., 1997. *Simulation of high speed filling*. Stress Engineering Services, Inc., Cincinnati, Ohio, 4–5, 9.

Pai M., Bermejo-Moreno I., Desjardins O., Pitsch H., 2009. Role of Weber number in the primary breakup of liquid jets in crossflow. *Center of Turbulence Research, Annual Research Briefs*, 145–158.

Ren J., Ouyang J., Yang B., Jiang T., Mai H., 2011. Simulation of container filling process with two inlets by improved smoothed particle hydrodynamics (SPH) method. *Int. J. Comput. Fluid Dyn.*, 25, 365–386. DOI: 10.1080/10618562.2011.603308.

Roberts S.A., Rao R.R., 2011. Numerical simulations of mounding and submerging flows of shear-thinning jets impinging in a container. *J. Non-Newtonian Fluid Mech.*, 166, 1100–1115. DOI: 10.1016/j.jnnfm.2011.06.006.

Sanjay V., Das A.K., 2017. On air entrainment in a water pool by impingement of a jet. *AIChE J.*, 63, 5169–5181. DOI: 10.1002/aic.15828.

Tomé M.F., Mckee S., Barratt L., Jarvis D.A., Patrick A.J., 1999. An experimental and numerical investigation of container filling with viscous liquids. *Int. J. Numer. Methods Fluids*, 31, 1333–1353. DOI: 10.1002/(SICI)1097-0363(19991230)31:8<1333::AID-FLD932>3.0.CO;2-R.

Van De Donk J., 1981. *Water aeration with plunging jets*. Ph.D. Thesis, TU Delft, the Netherlands, 168.

Venard J.K., Street R. L., 1975. *Elementary fluids mechanics*, 5^{th} edition, Wiley, New York. DOI: 10.1017/S002211 2063210124.

Wojtas K., Makowski Ł., Orciuch W., 2020. Barium sulfate precipitation in jet reactors: large eddy simulations, kinetics study and design considerations. *Chem. Eng. Res. Des.*, 158, 64–76. DOI: 10.1016/j.cherd.2020.03.019.

Wroński S., Pohorecki R., Siwiński J., 1979. *Przykłady obliczeń z termodynamiki i kinetyki procesów inżynierii chemicznej.* Wydawnictwo Naukowo-Techniczne, Warszawa, 307.

Zhu Y., Oğuz H., Prosperetti A., 2000. On the mechanism of air entrainment by liquid jets at a free surface. *J. Fluid Mech.*, 404, 151–177. DOI: 10.1017/S0022112099007090.

Zuritz C.A., Munoz Puntes E., Mathey H.H., Perez E.H., Gascon A., Rubio L.A., Carullo C.A., Chernikoff R.E., Cabeza M.S., 2005. Density, viscosity and coefficient of thermal expansion of clear grape juice at different soluble solids concentrations and temperatures. *J. Food Eng.*, Elsevier, Argentina, 1–7. DOI: 10.1016/j.jfoodeng.2004.10.026.

Received 21 April 2020
Received in revised form 13 May 2020
Accepted 14 May 2020